The effect of farmland on the surface water of the Aral Sea Region Using Multi-Source Satellite Data

Jiancong Shi [1, 2] , Qiaozhen Guo [Corresp., 1] , Shuang Zhao [1] , Yiting Su [3] , Yanqing Shi [1]

[1] school of geology and geomatis, Tianjin Chengjian University, Tianjin, China

[2] Taiyuan Design Research Institute Group Co., Ltd for Coal Industry, Taiyuan, China

[3] College of Geoscience and Surveying Engineering, China University of Mining and Technology-Beijing, Beijing, China

Corresponding Author: Qiaozhen Guo
Email address: gqiaozhen@tcu.edu.cn

Background: The improper land utilization has brought tremendous pressure on the surface water of the Aral Sea Region in the past decades. It was seriously hindered for construction of the Green Silk Road Economic Belt by the fragile environment. Therefore, it is of great necessity for environmental protection and social development to monitor the change of surface water in the Aral Sea Region. **Methods**: In this study, LandTrendr algorithm was used on Landsat time-series data to characterize the change in farmland on the Google Earth Engine platform. Based on multi-source data, the water area changes of the Aral Sea were extracted based on the Google Earth Engine, and the mean method was utilized to extract the changes in water level and water storage. Finally, a water-farmland coupling degree model was utilized to evaluate the impact of farmland changes on the surface water in the Aral Sea Region. **Results**: As a result, the change of farmland is as follows: the farmland area of the Aral Sea Region has abandoned 3129 km^2 from 1987 to 2019, with overall accuracy of 85.3%. The farmland change had increased the drainage downstream of the Amu Darya River and the Syr Darya River. It has led area of the Aral Sea to decrease each year continuously. The area of the Aral Sea shrank by 1606.36 km^2 per year from 1987 to 2019. Furthermore, Aral Sea's water level decreased by 0.13 m per year from 2003 to 2009. The amount of water storage in the Aral Sea Region also showed a downward trend from 2002 to 2016. There was a high-quality coupling coordination 0.903 relationship between surface water and farmland. It will increase the burden of water for people's normal daily life by the water loss resources caused by abandoned farmland. This study emphasized threat of unreasonable farmland management to surface water of the Aral Sea Region. The findings contributed for decision makers to formulating effective reasonable policies to protect surface water and use land of the Aral Sea Region. Meanwhile, the application of coupling degree model can provide a new method for

studying the connection of independent systems in the farmland, water, environment and more.

The Effect of Farmland on the Surface Water of the Aral Sea Region Using Multi-Source Satellite Data

Jiancong Shi[1,2], Qiaozhen Guo[1], Shuang Zhao[1], Yiting Su[3], Yanqing Shi[1]

[1] School of Geology and Geomatics, Tianjin Chengjian University, Tianjin, China
[2] Taiyuan Design Research Institute Group Co., Ltd for Coal Industry, Taiyuan, Shanxi, China
[3] College of Geoscience and Surveying Engineering, China University of Mining and Technology-Beijing, Beijing, China

Corresponding Author:
Qiaozhen Guo[1]
Jinjing Road, Xiqing District, Tianjin, 300384, China
Email address: gqiaozhen@tcu.edu.cn

Abstract

Background: The improper land utilization has brought tremendous pressure on the surface water of the Aral Sea Region in the past decades. It was seriously hindered for construction of the Green Silk Road Economic Belt by the fragile environment. Therefore, it is of great necessity for environmental protection and social development to monitor the change of surface water in the Aral Sea Region.
Methods: In this study, LandTrendr algorithm was used on Landsat time-series data to characterize the change in farmland on the Google Earth Engine platform. Based on multi-source data, the water area changes of the Aral Sea were extracted based on the Google Earth Engine, and the mean method was utilized to extract the changes in water level and water storage. Finally, a water-farmland coupling degree model was utilized to evaluate the impact of farmland changes on the surface water in the Aral Sea Region.
Results: As a result, the change of farmland is as follows: the farmland area of the Aral Sea Region has abandoned 3129 km^2 from 1987 to 2019, with overall accuracy of 85.3%. The farmland change had increased the drainage downstream of the Amu Darya River and the Syr Darya River. It has led area of the Aral Sea to decrease each year continuously. The area of the Aral Sea shrank by 1606.36 km^2 per year from 1987 to 2019. Furthermore, Aral Sea's water level decreased by 0.13 m per year from 2003 to 2009. The amount of water storage in the Aral Sea Region also showed a downward trend from 2002 to 2016. There was a high-quality coupling coordination 0.903 relationship between surface water and farmland. It will increase the burden of water for people's normal daily life by the water loss resources caused by abandoned farmland. This study emphasized threat of unreasonable farmland management to surface water of the Aral Sea Region. The findings contributed for decision makers to formulating effective reasonable policies to protect surface water and use land of the Aral Sea Region. Meanwhile, the application of coupling degree

40   model can provide a new method for studying the connection of independent systems in the
41   farmland, water, environment and more.

Introduction

43   As the essential water resources in the Aral Sea Basin and even in Central Asia, the Aral Sea
44   could primarily ensure the stability of the surface water to be maintained (Micklin, 1988).
45   However, the area of the Aral Sea is currently only one-tenth of that in 1960 (Wu et al., 2020). As
46   impacted by the rapid shrinking of the Aral Sea, the surface water of the Aral Sea Basin has been
47   severely decreased (Eleni et al., 2020). The shrinking surface water caused land desertification and
48   land salinization (Parajuli et al., 2017), thereby seriously endangering the development of society.
49   Accordingly, it is essential for protection of the surface water and regional development to reveal
50   the root cause of the Aral Sea's shrinkage.
51   The Aral Sea Basin refers to a severely arid area with annual precipitation of less than 300
52   mm (Elena, 2014). Thus, the level of the Aral Sea is determined by the inflow of two feeding
53   rivers, the Amu Darya and the Syr Darya (Philippe et al., 2007). The two rivers originate from the
54   melting of snow in the mountains of southeast of the Aral Sea Basin (Micklin, 2016). Scholars
55   have carried out researches on the upstream of Amu Darya and Syr Darya, as presented below.
56   Valentina et al. found that the snow depth in the rivers' (e.g., the Amu Darya and the Syr Darya)
57   source tended to decrease after 1965, whereas the runoff downstream has been declining
58   (Valentina et al., 2009). Hagg et al. considered that the runoff of the upper reaches in the Amu
59   Darya River would gradually increase (Hagg et al., 2007). In a word, considerable researches
60   indicated a downtrend of snow depth in the source of the Amu Darya River and the Syr Darya
61   River, whereas the runoff downstream has been declining (Annina et al., 2012; Wang et al., 2016).
62   The above studies show that the upstream runoff of Amu Darya and Syr Darya increases each year,
63   which is contrary to the shrinkage of the Aral Sea. At the same time, researchers have found that
64   the shrinkage of the Aral Sea is directly related to the reduction of runoff downstream of rivers
65   (Shi et al., 2021; Micklin, 2007). Therefore, this study will focus on the downstream area of rivers
66   near the Aral Sea.
67   Over the past decades, unreasonable land utilization led to the decline of downstream runoff
68   in the Amu Darya River and the Syr Darya River, which directly caused the shrinking of the Aral
69   Sea (Christopher et al., 2016). Primarily, neighbouring countries used a lot of lands to plant
70   farmland, and have done many radical measures to increase the value of agricultural output. For
71   instance, the former Soviet Union built the channel with 500 km in the Amu Darya River area and
72   the Syr Darya River area in 1960. Such a project took one-third of the water in rivers downstream
73   to farmland (Conant, 2006). The mentioned measure altered the rain-fed irrigation mode of
74   farmland in the Aral Sea Basin (Micklin, 2007). By 2010, the irrigated area of the Aral Sea Basin
75   was 7,895,600 ha, taking up 78.6% of planted land (data from the Central Asia Water Resources
76   Network: www.cawater-info.net). Inefficient irrigation systems and terrible management of land
77   utilization triggered the increase in water withdrawn from rivers. Thus, surface water protection
78   requires the exploration of the farmland variations in the Aral Sea Basin. Several studies have been
79   conducted on the surface water variations attributed to irrigation. For instance, Jin et al.

80 investigated human irrigation-induced hydrological variations in the Aral Sea Basin by multiple
81 satellite data (Jin et al., 2017). Fabian et al. mapped abandoned farmland to support surface water
82 protection in Kyzyl-Orda, Kazakhstan (Fabian et al., 2015). However, existing studies could not
83 determine a quantitative model to assess the impact of farmland changes on surface water.
84 Accordingly, it is of great necessity to establish a method to assess the effect of farmland changes
85 on surface water.

86   For the complicated political issues and poor physical accessibilities of the Aral Sea Region,
87 there are severe limitations in collecting data required for large-scale and long-term change
88 detection and analyses (Fabian et al., 2015). As an alternative, remote sensing technology,
89 exhibiting the advantages in data of effective coverage of long-term span and multi-time scale, has
90 been extensively employed in natural disaster early warning, eco-environmental protection,
91 farmland protection, dynamic analysis of land use, social development, etc. (Tewkesbury et al.,
92 2015; Li et al., 2003; Saha et al., 2019). Alka et al. used multi-source data to explore inter-annual
93 water storage variations in the Aral Sea (Singh et al., 2012). Jin et al. adopted multiple satellite
94 data to view environmental variations around the Aral Sea (Jin et al., 2017). At present, remote
95 sensing technology has become an essential measure of long-term monitoring variations in surface
96 water in large areas (Singh et al., 2012). However, the above researches are difficult to characterize
97 the impact of farmland on the surface water quantitatively. Thus, this study combined the
98 comprehensive variations of water and farmland changes to explore the internal relationship
99 between the surface water and farmland based on multi-source data.

100   The water area, water level and surrounding water storage of the Aral Sea act as critical
101 indicators to characterize the hydrological variations in the Aral Sea. Multi-source data efficiently
102 supports extracting the comprehensive variations of water. The LandTrendr (Landsat-based
103 Detection of Trends in Disturbance and Recovery) algorithm can capture both long-term gradual
104 and short-term drastic variations (Gorelick et al., 2017). Moreover, Kennedy et al. encapsulated
105 the LandTrendr on the GEE platform to consume considerable computation time in continuous
106 change detection, (Kennedy et al., 2018). Moreover, it has been broadly applied in most fields of
107 change detection (Zhu et al., 2019). The coupling degree model is capable of reflecting the degree
108 of association between multiple subsystems.

109   This study aimed to examine the surface water attributed to land utilization change of the Aral
110 Sea Region. The specific steps are as follows: Firstly, the LandTrendr algorithm was run on
111 Landsat time-series of the GEE platform to detect the land utilization change modes. Second, the
112 variations of water area, water level and water storage were detected using multi-source data
113 (Landsat, ICESat, GRACE). Lastly, to explore the effect of farmland changes on the surface water,
114 the variations of water (water area, water level and water storage) and farmland were combined to
115 build a water-farmland coupling degree model. The mentioned efforts can provide explicit
116 cognitions regarding the effect of farmland on surface water. Furthermore, it can provide practical
117 implications for agricultural governance, water protection and   surface water balance.

118

119 **Materials & Methods**

120 2.1 Study Area

121   The Aral Sea Region is located on the border between northwest Uzbekistan and southwest
122 Kazakhstan. It covers 130,000 km^2, and includes North Aral, East Aral, West Aral and irrigated
123 farmland of the Aral Sea Region (Figure 1). This is a typical arid area with an average annual
124 temperature of 11.62 ℃ and precipitation of 126.26 mm.

125

126   **Figure 1**. Research scope: (a) general location in the Aral Sea Basin and the Central
127   Asia; (b) 1987 land-use classification from Google Earth Engine (GEE) imagery

128 2.2 Data Preparation

129 2.2.1 Landsat data and Pre-processing

130   Landsat surface reflectance data (Landsat5, Landsat7 and Landsat8) were collected from
131 1984 to 2019 on GEE platform. This study used the FMASK and neighboring position filling to
132 improve extraction accuracy to remove the mentioned poor-quality (snow/ice, clouds, building
133 shadows and scan-line corrector (SLC)-off gaps) images (Zhu et al., 2012). Accordingly, the
134 Landsat surface reflectance dataset was produced for our study area from 1987 to 2019 (A-LSTC).
135 Lastly, the dataset (YA-LSTC) was synthesized into annual images from the A-LSTC (June 1 to
136 September 1). The normalized vegetation index (NDVI) was introduced to the dataset as a new
137 band (Tucker, 1979).

$$NDVI = \frac{\rho_{nir} - \rho_r}{\rho_{nir} + \rho_r} \tag{1}$$

138 Where ρ_{nir} and ρ_r are the near-infrared band and red band in Landsat.

139 2.2.2 ICESat satellite altimetry data

140   The ICESat mission was initiated in January 2003 and ended in February 2010 by National
141 Aeronautics and Space Administration (NASA) (Schutz et al., 2005). The Geoscience Laser
142 Altimeter System (GLAS) on ICESat has provided global measurements of polar ice sheet mass
143 balance, cloud and aerosol heights, land topography and vegetation characteristics with a surface
144 sampling diameter of 70 m as well as a spacing of 172 m (Zwally et al., 2008). ICESat/GLAS level
145 2 altimetry product (GLA14) consists of global land surface elevation data (Kwok et al., 2004).
146 The GLA14 has been broadly introduced in lake water level and land elevation and have reflected
147 accuracy over 10 cm (Zhang et al., 2011). Thus, the GLA14 can precisely contribute to the surface
148 elevation. The GLA14 from 2003 to 2009 were collected to extract the water level change in the
149 Aral Sea.

150 2.2.3 GRACE Data

151   The Gravity Recovery and Climate Experiment (GRACE) mission was launched in March
152 2002 and ended in October 2017 by NASA. The water mass variations were considered a change

153   of Earth's gravity by GRACE (Jin et al., 2017). Most gravity signals after de-noising of GRACE
154   reflect variations in water storage (Chen et al., 2019; Swenson et al., 2007). However, the orbital
155   altitude and resolution of GRACE limited the effective research range ($< 200,000$ km^2) (Singh et
156   al., 2012). Thus, the original research range was extended to 230,000 km^2. Though the study area
157   is less than 230,000 km^2, it can be assumed that the mass variations on long-time scales come from
158   the long-term storage change of water of the Aral Sea Region. Thus, the GRACE data was
159   processed in the GEE platform from 2002 to 2016 (research range between June and September
160   each year).

161   2.3. Detection Algorithm

162

163   **Figure 2.** Research Method: (a) The method of farmland change detection; (b) The method of
164   water change detection; (c) The method coupling degree model.

165   2.3.1. Detection Algorithm of Farmland Change

166   LandTrendr (Landsat-based Detection of Trends in Disturbance and Recovery) algorithm is
167   an approach to extract the spectral trajectories of land surface from Landsat time-series stacks
168   (Watts et al., 2014). This algorithm can reflect farmland variations by detecting the temporal-
169   spectral trajectory of each pixel. The input of every pixel for the algorithm is a time series with
170   one spectral value or index. This algorithm also needs to set parameters, such as noise-induced
171   spikes (outliers), potential vertices (breakpoints), fitting trajectories, and the optimal number of
172   segments (Watts et al., 2014).
173   LandTrendr algorithm on the GEE platform was used to detect the farmland change in the
174   Aral Sea Region (Figure 2-(a)). Before running this algorithm, the features of farmland variations
175   were analyzed, tested different combinations of parameter values. The NDVI was determined as
176   the spectral index, and other parameters were calculated (Table S1). NDVI of farmland ranged
177   from 0.45 to 0.69 in the Aral Sea Region and plummeted after abandonment to range from 0.2 to
178   0.3. Thus, NDVI of abandoned farmland was set between 0.2 and 0.3. The mentioned thresholds
179   were adopted to detect the change patterns of farmland, the change time of occurrence and end,
180   and duration.
181   **Table S1.** Operating parameters of LandTrendr

182

183   2.3.2. Detection Algorithm of Waters Change

184   Via the GEE platform, the random forest algorithm was adopted to detect the variation of
185   water area (Figure 2-(b)). Random forest is a machine learning algorithm that is complies with the
186   decision tree. This algorithm uses CART clustering for prediction and classification (Breiman,
187   2001). Two primary parameters should be set before implementing the random forest algorithm.
188   To be specific, the first refers to the number of splitting times (mtry) of the branch tree in each

189   model. This parameter should be set as the square root value of variables and 2 times or 1/2 of the
190   prediction's open value. In this paper, the variables specifically refer to the bands of remote sensing
191   images (Table S2). The second refers to the number of generated trees (ntree) in model operation,
192   and the amount of model calculation is proportional to the value of ntree. The ntree was set as 500
193   because it will be pretty obvious with a bit of tinkering that the predictions from the model will
194   not change much after this value.
195   The accuracy of model depends more on quality of training samples. Therefore, we selected
196   200 pixels representing water and another 200 pixels representing non-water based on Landsat
197   imagery. In order to access accuracy of results, we visually examined all selected pixels (from
198   1987 to 2019) and used high-spatial-resolution Google Earth imagery for further manual
199   interpretation of land cover (Figure 3). Therefore, we determined and recorded whether and when
200   water pixels change occurred.
201
202   **Table S2.** Variables of Random Forest Algorithm
203
204   **Figure 3**. Examples areas of water change and farmland change near the Syr Darya and the Amu
205   Darya. Figures a1 and a2 represent the water change years 2009 and 2019; Figures b1, b2, b3
206   represent the water change years 2009, 2016 and 2019.
207
208   The ICESat data was adopted to analyze the alteration in water level in the Aral Sea. At first,
209   the data format of GLA14 was converted. Second, GLA14 was adopted to extract the water level
210   of the Aral Sea (Eq. 2). Lastly, the water volume was calculated according to the alteration in water
211   level and the variation of water area of the Aral Sea (Eq. 3). Meanwhile, researchers compared
212   ICESat data with airborne LiDAR data and DEM from GPS data. The error of ICESat data is less
213   than 3 cm (Kurtz et al., 2008; Fricker, 2005).

$$WL_T = \frac{\sum_{i=1}^{n} wl}{n} \tag{2}$$

$$WV = WL_T * WA \tag{3}$$

214   Where WL_T is mean water level. wl is the land elevation of every ICESat point. WV is water
215   volume. WA is water area.
216   The GRACE dataset was used to extract the equivalent water height (EWH). The data
217   contained in this dataset are units of "Equivalent Water Thickness" which represent the deviations
218   of mass in terms of the vertical extent of water in centimeters (Watkins et al., 2015). The EWH
219   was processed at NASA Jet Propulsion Laboratory. Actually, this dataset was produced by three
220   institutions: CSR (U. Texas / Center for Space Research), GFZ (German Research Center for
221   Geosciences), and JPL (NASA Jet Propulsion Laboratory). However, since each institution
222   independently produces the coefficients, the results may be slightly different. And the mass change

223   maps of the three institutions have typically suffered from poor observability of east-west
224   gradients, resulting in "N-S stripes" that are conventionally removed via empirical smoothing
225   and/or "destriping" algorithms. In order to overcome these limitations, Watkins et al., developed
226   GRACE(-FO) mass concentration (mascon)solutions (Watkins et al., 2015; Wiese et al., 2016;
227   Landerer et al., 2020). The solutions allow for convenient application of a priori information
228   derived from near-global geophysical models to prevent striping. Significantly, over the land,
229   mascon solutions have more excellent resolution for smaller spatial regions, in particular when
230   studying secular signals. Meanwhile, for different application scenarios, the dataset has its
231   advantages. For instance, it is more suitable for water, ice mass, and ocean bottom pressure mass
232   change application to use JPL mascon (Watkins et al., 2016; Landerer et al., 2020). Therefore, JPL
233   data, which have been processed by the GRACE(-FO) mascon solutions, were used in this paper.
234   And the measurement accuracy of GRACE data is credible (5000km wavelength: 0.001mm;
235   500km wavelength: 0.01mm) (Zheng et al., 2009). Water storage variation in the Aral Sea Region
236   was analyzed (Eq. 4).

$$WS = EWHT * A \tag{4}$$

237   Where EWHT is the equivalent water height from GRACE dataset; WS is water storage; A
238   is the area of study region.

2.4. Accuracy Assessment

240   Two hundred pixels were selected to build a confusion matrix (CM) to assess the accuracy
241   of the five surface features in 1987 (i.e., water, farmland, desert, shoal and irrigation land).
242   Meanwhile, we visually examined all surface features by high-spatial-resolution Google Earth
243   imagery. The overall accuracy, user accuracy, and producer accuracy for each feature were
244   concluded following the indexes defined by Foody and Green (Congalton et al., 1993; Foody,
245   2002). Two hundred validating pixels were selected to represent the stable area of farmland. In
246   addition, another 200 validating pixels represent the various area of farmland for each change
247   mode. The stable area refers to the pixels that remain unchanged as farmland for years. While the
248   various area represents the changed farmland pixels during the whole study period. The 20% pixels
249   of training samples in water extraction were adopted to produce a CM to access the accuracy of
250   water extraction results.

2.5. Water-Farmland Coupling Degree Model

252   The coupling degree model originated from the coupling coefficient model in physics.
253   Farmland and surface water were combined to build the water-farmland coupling degree model to
254   explore the impact of farmland on surface water. In such a model, four indicators were selected
255   related to surface water and farmland (Figure 2-(c)). At first, every indicator was normalized, and
256   then the entropy method was used to determine their weight. The index matrix is $X = (x_{ab})_{i \times j}$
257   (where i is the evaluation index; j is the index, and x_{ab} is the b-th index of the a-th sample,). The
258   coupling degree model (C) is as follows (Chang, 2018).

$$C = \left\{ \frac{f_1(x) * \cdots * f_i(x)}{\left| \frac{f_1(x) + \cdots + f_i(x)}{i} \right|_i} \right\}^{1/i} \tag{6}$$

$$f_i(x) = \sum_b^j w_b x_b \tag{7}$$

259   Where $f_i(x)$ is the comprehensive evaluation function of subsystem; w_b is the weight of each
260   index; x_b is each index; i is the number of subsystems to be access. There are two subsystems which
261   need to be evaluated, so $i = 2$. ($C \in [0,1]$). If the C value is closer to 1, it will mean that the
262   subsystems are more related and coordinated (Congalton et al., 1993).
263

264   **Results**

265   3.1. Accuracy Assessment
266

267   The CM for the classification of 1987 imagery (Table S3) revealed that the overall accuracy
268   (OA) reached over 90%. The user accuracy (UA), and producer accuracy (PA) for each class
269   mainly were more than 86%. The accuracy of farmland is less than 90%. The reasons are elucidated
270   below. There were considerable irregular water bodies and farmland in irrigated land of the Aral
271   Sea Region; thus, the farmland often tended to mix with water and Irrigation land. Moreover, some
272   sparse vegetation was planted in the irrigation land. Thus, it was difficult to distinguish by
273   employing Landsat images with a spatial resolution of 30m. However, the overall accuracy reached
274   92.1%, suggesting the random forest model's capability. A similar method was used to assess the
275   accuracy of extraction of water area in the Aral Sea from 1987 to 2019. The accuracy of extraction
276   of water area reached over 90%, demonstrating the credibility of the results.
277   **Table S3.** Confusion matrix for the 1987 classified image.
278

279   Table S4 show the farmland detection accuracy of abandon and replanting by LandTrendr.
280   The overall accuracy of 85.3% was low for abandoned farmland for the mixture of abandoned
281   farmland and sparse planting. For the replanting, the PA, UA, and OA are above 80%. Thus, it is
282   sufficient for farmland to detect the change model. In summary, the OA of abandoned farmland
283   change detection was more than 85%, demonstrating the detection method's reliability based on
284   the LandTrendr.
285   **Table S4.** Confusion matrix for the change detection of abandoned farmland.
286

287 3.2. Temporal and Spatial Variations of Farmland

288 The distribution of abandoned farmland, in the Aral Sea Region during 1987-2019, was
289 rendered the disturbance map with a gradient (Figure 4) according to the occurrent years. The
290 abandoned region was mainly diffused around the Syr Darya and the Amu Darya, especially
291 around the Amu Darya (Table S5). Within 9 km of these Draya rivers, the percentage of abandoned
292 farmland reached 59.96% from 1987 to 2019. Overall, 3129 km^2 of farmland was abandoned. The
293 annual change peaked between 1987 and 1993 (Table S6), after which percentage of abandoned
294 farmland decreased under 3% from 2002 to 2016 (Table S6). However, the percentage of
295 abandoned farmland was elevated to 5.7% in 2017 (Table S6), which resulted in the plummet of
296 water volume in the Aral Sea.

297

298 **Figure 4.** Year of abandoned farmland in the Aral Sea Region with two areas shown in detail: (a)
299 Around the Syr Darya River; (b) Around the Amu Darya River.
300
301 **Table S5.** Area of Abandoned Farmland near the Amu Draya and the Syr Draya
302
303 **Table S6.** Area of Abandoned Farmland in the Aral Sea Region
304

305 3.3. Waters Variations of the Aral Sea Region

306 The Aral Sea has been shrinking at 1606.36 km^2 per year from 1987-2019. In 2019, the area
307 of the Aral Sea took up only 15.6% of its size in 1987 (Figure 5). With an annual decrease of
308 1306.18 km^2, the East Aral (820.22 km^2) had almost dried up by 2019. The area of the East Aral,
309 in 2019, only accounted for 1.92% in 1987. On the contrary, as impacted by the construction of
310 the Dike Kokaral dam in 2005, the North Aral showed a weak expansion trend with an average
311 annual growth of 10.05 km^2. The area of North Aral rose to 4658.773 km^2 in 2019. Kazakhstan
312 Government built the Kokaral dam at the junction of the North Aral and East Aral (Figure 5). In
313 order to keep the water level of North Aral and environment stable, the water flow from North
314 Aral to East Aral was artificially reduced. Though this policy effectively prevented the loss of
315 North Aral, it also reduced the water flowing into East Aral. Such a dam aggravated the dry-up of
316 East Aral. The West Aral is small and far from the irrigated area. Accordingly, the West Aral had
317 shrunk more minor than the East Aral at 314.83 km^2 each year.

318

319 **Figure 5.** Change of the Aral Sea area from 1987 to 2019: (a) the spatial distribution; (b) the
320 temporal distribution.
321 Likewise, the water level of the Aral Sea tended to decrease. The curve of the water level of
322 the North Aral significantly ascended as impacted by the construction of the dam (Figure 6). The
323 water level of the North Aral was elevated near 0.32 m per year from 2003 to 2009. In the East
324 Aral, the water level drastically declined at 0.5 m per year. Moreover, the East Aral was only 0.05

325 m in 2019. Compared with the East Aral, declining West Aral was lower as impacted by its smaller
326 range and farther from the irrigated area. To be specific, the water level of the West Aral decreased
327 at 0.4 m per year and dropped to 2.1 m in 2019.

328

329   **Figure 6.** Change of the Aral Sea water level from 2003 to 2009.

330   Figure 7 illustrates the water mass change of the GRACE analysis in the study area. The curve
331 of equivalent water height shows a downward trend from 2002 to 2016. The change of equivalent
332 water height is same as the water level. The water mass was overall declining, marking a decrease
333 by 0.97 km^3 each year. The decrease in water mass represented the descending of water storage,
334 such as the Aral Sea, rivers, reservoirs and groundwater.

335

336   **Figure 7.** Mass change of the Aral Sea Region from 2002 to 2016.

337 3.4. Construction of Water-Farmland Coupling Degree Model

338   According to the results of this study regarding water and farmland in the Aral Sea Region,
339 three indexes were selected to build a comprehensive evaluation index system (Table S7). This
340 system included two subsystems (surface water system, farmland system). Water subsystem had
341 two evaluation indexes, and farmland subsystem had one evaluation index (Table S7).

342   The entropy method was adopted to calculate the weight of each index. According to the
343 mentioned weights, the coupling degree was obtained between the two subsystems from 2003 to
344 2009. In addition, the results indicated that the annual coupling degree value was above 70%, and
345 the average coupling degree reached 0.903 (Table S8). By the criterion of coupling degree (Table
346 S9) (Chang, 2018), only 2003 and 2005 pertain to intermediate level coupling coordination. Other
347 years belong to high-quality coupling coordination. In addition, the average coupling degree
348 belongs to the high-quality coupling coordination. The mentioned coupling degree results
349 suggested that the greater coupling degree between the two subsystems, and farmland changes
350 affected the variations of surface water in the Aral Sea Region.

351   **Table S7.** Comprehensive evaluation index system of water and farmland coupling
352   degree.

353

354

355   **Table S8.** Weight of every index, coupling degree value of every year and average
356   coupling degree value.

357

358   **Table S9.** Criteria for Coupling Coordination Type

359

360 **Discussion**

361 4.1. Benefits of Methods

362   The results shown that, the loss of water by abandoned farmland will increase the burden of
363 normal water use. During the past years, many scholars were committed to analyzing the reasons
364 for the decrease of surface water in the Aral Sea Region. Compared with previous researches, our
365 work has similarities and differences. For similarities, the surface water loss was caused by
366 improper irrigation management. On the contrary, our research was from the perspective of
367 farmland abandonment. Few studies have analyzed the loss of water caused by abandoned
368 farmland. They were analyzed effect of land water storage on surface water (Jin et al. 2017;
369 Gaybullaev et al, 2012; Parajuli et al. 2017).

370   The coupling degree model was used for the first time to monitor the effect of farmland on
371 the surface water of the Aral Sea Region. Most previous researches regarded farmland and surface
372 water as independent objects, which could not acquire the natural connection between them.
373 Therefore, changes in farmland and surface water were put into a quantifiable system that can be
374 used to explore the substantial impact of farmland changes on the surface water. According to the
375 result, the coupling degree model showed good applicability in this field. In addition, it could
376 provide a new method for the internal connection between farmland, surface water, and ecology
377 in the Aral Sea Region and even the Aral Sea Basin.

378

379 4.2. Effect of Abandoned Farmland on Surface Water in Aral Sea Region

380   The abandoned farmland will cause a lot of surface water loss. The main reason is that
381 irrigation canals of abandoned farmland are not blocked because of the negligence of management.
382 It directly led to majority of the water was being soaked up by the desert and blatantly loss
383 (Ibragimov et al, 2007; Maksud et al, 2016; Jabbarov et al, 2013). According to the results of
384 section 3.2, we extracted the area of abandoned farmland (Table S6). The area of abandoned
385 farmland reached per year 97.843 km^2. And the abandoned farmland will cause a lot of water
386 waste. Farmland in Aral Sea Region is concentrated on planting cotton, wheat and rice
387 (Chapagainet al., 2005). Table S10 shows that wheat is the thirstiest crop. And the water use
388 efficiency of cotton is the lowest (0.451*108kg/km^3). Table S11 shows the crop production in
389 precious decades.

390

391       **Table S10.** Crop Water use efficiency in Aral Sea Region.

392

393        **Table S11.** Crop production in the Aral Sea Region.

394

395   Based on the above results, the loss volume of water loss by abandoned farmland can be
396 extracted. If all the abandoned farmland were used to plant cotton in the past few years, the water
397 loss would reach 0.028 km^3 every year (Table S12). According to the current distribution of
398 available water per capita from the World Bank (Uzbekistan, 2596 m^3/ per person / annually;

399   Kazakhstan, 1943 m³/ per person / annually), the water loss can provide annual domestic water for
400   tens of thousands of people in the Aral Sea Region. The specific numbers are as follows:
401   Kazakhstan are 14410 persons, and Uzbekistan are 10785 persons. Therefore, abandoned farmland
402   caused additional loss of normal domestic water for people in the Aral Sea Region.

403

404   **Table S12.** Water Consumption for Planting Cotton in Abandoned Farmland.

405

406   The previous researches gave us much inspiration. Micklin macroscopically analyzed the
407   reason and effect of water changes in the Aral Sea (Micklin, 2010). Yoshihiro et al. found nearly
408   100% return flows of the applied irrigation water in the Aral Sea Drainage Basin (Yoshihiro et al.,
409   2007). Cretaux et al. analyzed effect of groundwater on the hydrological water budget of the Aral
410   Sea by remote sensing data (Cretaux et al., 2013). Compared with above researches, our
411   contributions are as follows:
412   1. Based on the coupling degree model, we quantitatively characterized the effect of
413   farmland changes on surface water.
414   2. The coupling degree model was used for the first time to study the effect of farmland
415   changes on surface water. We believe that this attempt will help broaden the thinking of
416   researchers in the fields of remote sensing, environment and more. They can connect
417   independent systems through the coupling degree model.
418   3. The effect mechanism was analyzed on surface water changes by calculating the amount
419   of water loss in abandoned farmland. Moreover, the normal domestic water for people
420   caused by water loss was analyzed.

421

422   4.3. Limitations of Research

423   At first, vegetation indices can reduce other factors' impacts in monitoring land cover change
424   (Zhang et al., 2013). The NDVI can reduce the influence of external environmental factors on the
425   surface reflectance to some extent. Previous studies indicated that the accuracy of NDVI in
426   detecting farmland is better than others (Tong et al., 2017). However, due to the disturbance by
427   other vegetation in the arid region, using NDVI to the LandTrendr algorithm has some limitations
428   (Watts et al., 2014). A typical example is that the sparse vegetation of the Aral Sea Region
429   generated the same NDVI signal with farmland and affected the detection results. Therefore, it is
430   necessary to add additional indices to improve accuracy.
431   Secondly, the data on water level and water storage cannot match the water area's time series.
432   However, this fusion of data yet offers valuable and unique information on the surface water.
433   Simultaneously, in the next step of our research, we need to improve data integrity of the surface
434   water.

435   **Conclusions**

436   In this study, the farmland variations were detected by using LandTrendr algorithm based on
437   the GEE platform. Subsequently, multi-source data (Landsat, ICESat, GRACE) were employed to

438   extract the variations of water area, water level, water storage in the Aral Sea Region. Given the
439   mentioned results, the Water-Farmland assessment was developed. Such a system assessed the
440   impact of farmland on surface water in the Aral Sea Region. The specific results are elucidated
441   below:

442   Throughout the research, the abandoned farmland areas covered 98 km^2 per year. The overall
443   accuracy of abandon took up 85.3%. There was most abandoned farmland near the rivers (the Amu
444   Darya River and the Syr Darya River) from 1987 to 2019 of the Aral Sea Region (Section 3.2).
445   The abandon of farmland had triggered a massive loss of water resources of the Aral Sea Region.

446   Second, the Aral Sea shrank by 1606.36 km^2 per year from 1987 to 2019, in which the East
447   Aral shrank most seriously. Furthermore, the Aral Sea's water level was down-regulated by 0.13
448   m per year from 2003 to 2009, especially the East Aral. However, as impacted by the construction,
449   Dike Kokaral dam in 2005, the water level and area curves in the North Aral started to elevate
450   after 2005. Moreover, the amount of water storage in the Aral Sea Region declined from 2002 to
451   2016.

452   The coupling degree model overall considers the variations in surface water and farmland. In
453   addition, the average coupling degree value exhibits high-quality coupling coordination,
454   demonstrating that farmland changes significantly impact the surface water. Meanwhile, the
455   volume of water loss by abandoned farmland caused additional loss of normal domestic water for
456   people. Such a method can be referenced to investigate the effect of farmland on surface water or
457   other fields. Moreover, the mentioned results are capable of helping relevant researchers gain
458   insights into the effect of variations in farmland on surface water deterioration in this region, and
459   offer sufficient support for subsequent governance and research.
460

461   **Acknowledgements**
462

463   **References**

464   Annina, S., Tobias, B., Markus, S., Olga, S. and Martin, B. 2012. Climate change impacts on
465   glaciers and runoff in Tien Shan (Central Asia). *Nature Climate Change*, *2*(10), 725–731.
466   doi:10.1038/nclimate1592

467   Breiman, L. 2001. Random Forests. *Machine Learning*, *45*(1), 5–32.
468   doi:10.1023/A:1010933404324

469   Chang, Y. M. 2018. System coupling model and evaluation of water re-sources environment and
470   urban eco-economy. *Water Resources and Power,36*: 55–58.

471   Chapagain, A.K., R. Gautam, and A.Y. Hoekstra. 2005. "The Water footprint of cotton
472   consumption," UNESCO- IHE, The Institute of Water Education.

473   Chen, H., Zhang, W. C., Ning, Nie, N. and Guo, Y. D. 2019. Long-term groundwater storage
474   variations estimated in the Songhua River Basin by using GRACE products, land surface
475   models, and in-situ observations. *Science of the Total Environment*, *649*, 372–387.
476   doi:10.1016/j.scitotenv.2018.08.352

477 Christopher, C., Sarsh, S. S., Fabian, L., Denis, S. and Heiko, P. 2016. Cropping intensity in the
478 Aral Sea Basin and its dependency from the runoff formation 2000–2012. *Remote Sensing*, *8*(8),
479 630. doi:10.3390/rs8080630

480 Conant, E. 2006. Return of the Aral Sea. *Discover*.

481 Congalton, R.G. and Green, K. 1993. Practical look at the sources of confusion in error matrix
482 generation. Photogramm. Eng. Remote Sens, *59*(5), 641–644.

483 Cretaux, Jean-François, René Letolle, and Muriel Bergé-Nguyen. 2013 "History of Aral Sea
484 level variability and current scientific debates." *Global and Planetary Change, 110*: 99-113, doi:
485 10.1016/j.gloplacha.2013.05.006.

486 Elena, L. 2014. A multi-scale assessment of human vulnerability to climate change in the Aral
487 Sea basin. *Environmental Earth Sciences*, *73*(2), 719–729. doi:10.1007/s12665-014-3104-1

488 Eleni, F., Maria, T., Lena, H., Antonis, A., Rene, H., Kathrin, W. and Charalampos, V. 2020.
489 Water-related ecosystems' mapping and assessment based on remote sensing techniques and
490 geospatial analysis: The SWOS national service case of the Greek Ramsar sites and their
491 catchments. *Remote Sensing of Environment*, *245*, 111795. doi: 10.1016/j.rse.2020.111795

492 Fabian, L., Elisabeth F., Iskandar, A., Christopher, C. and John P.A. 2015. Mapping abandoned
493 agricultural land in Kyzyl-Orda, Kazakhstan using satellite remote sensing. *Applied Geography*,
494 *62*, 377–390, doi: 10.1016/j.apgeog.2015.05.009

495 Foody, G.M. 2002. Status of land cover classification accuracy assessment. *Remote Sensing of
496 Environment*, *80*(1), 185–201. doi:10.1016/s0034-4257(01)00295-4

497 Fricker, H. A. 2005. Assessment of ICESat performance at the salar de Uyuni, Bolivia.
498 *Geophysical Research Letters*, 32(21): L21S06, doi: 10.1029/2005GL023423.

499 Gaybullaev, B.; Chen, S.C.; Gaybullaev, D. 2012. Changes in water volume of the Aral Sea after
500 1960. Appl*ied* Water Science, 2: 285–291. doi: 10.1007/s13201-012-0048-zGorelick, N.,
501 Hancher, M., Dixon, M., Ilyushchenko, S., Thau, D. and Moore, R. 2017. Google Earth Engine:
502 Planetary-scale geospatial analysis for everyone. *Remote Sensing of Environment*, *202*, 18–27,
503 doi: 10.1016/j.rse.2017.06.031

504 Hagg, W., Braun, L. N., Kuhn, M. and Nesgaard, T. I. 2007. Modelling of hydrological response
505 to climate change in glacierized Central Asian catchments. *Journalof Hydrology*, *332*(1-2), 40–
506 53. doi: 10.1016/j.jhydrol.2006.06.021
507 Ibragimov, N., Steven R. E., Yusupbek E., Bakhtiyor S. K., Lutfullo M., John P.A. L. 2007.
508 Water Use efficiency of irrigated cotton in Uzbekistan under drip and furrow. *Agricultural Water
509 Management*, 90(1-2): 112-120. doi: 10.1016/j.agwat.2007.01.016
510 Jabbarov, Eshchanov, Nurmetov, Alexandra L., Margaret S., John P.A. L. 2013. Canal lining to
511 increase water use efficiency and remediate groundwater levels in Khorezm Uzbekistan, Central
512 Asia. *International Journal of Agriculture: Research and Review*, 3: 742-750. doi:
513 10.1039/DT9960002261

514 Jin, Q. J., Wei, J. F., Yang, Z. L. and Lin, P. R. 2017. Irrigation-Induced Environmental Changes
515 of adjacent the Aral Sea: An Integrated View from Multiple Satellite Observations. *Remote
516 Sensing*, *9*(9), 900. doi:10.3390/rs9090900

517 Kennedy, R.E., Yang, Z. Q., Gorelick, N., Braaten, J., Cavalcante, L., Cohen, W.B. and Healey,
518 S. 2018. Implementation of the LandTrendr Algorithm on Google Earth Engine. *Remote*
519 *Sensing*, *10*(5), 691. doi:10.3390/rs10050691

520 Kurtz, N., T. Markus, D. Cavalieri, W. Krabill, J. Sonntag, Jeffrey A. Miller. 2008. Comparison
521 of ICESat Data with Airborne Laser Altimeter Measurements Over Arctic Sea Ice. *IEEE*
522 *Transactions on Geoscience and Remote Sensing*, *46*(7):1913-1924.
523 doi:10.1109/TGRS.2008.916639.

524 Kwok, R., Zwally, H. J. and Yi, D. H. 2004. ICESat observations of Arctic sea ice: A first look.
525 *Geophysical Research Letters*, *31*(16), L16401. doi:10.1029/2004gl020309

526 Landerer, F. W., Flechtner, F. M., Save, H., Webb, F. H., Bandikova, T., Bertiger, W. I.,
527 Bettadpur S V, Byun S H, Dahle C, Dobslaw H, Fahnestock E, Harvey N, Kang Z, Kruizinga G
528 L. H., Loomis Bryant D., Mccullough C, Murböck M, Nagel, P, Paik M, Pie N, Poole S,
529 Strekalov D, Tamisiea M E., Wang F, Watkins M M., Wen H Y, Wiese D N., Yuan D N. 2020.
530 Extending the global mass change data record: GRACE Follow-On instrument and science data
531 performance. *Geophysical Research Letters*, *47*(12), doi:10.1029/2020GL088306.

532 Li, J. and Narayanan, R. M. 2003. A Shape-Based Approach to Change Detection of Lakes
533 Using Time Series Remote Sensing Images. *IEEE Transactions on Geoscience*
534 *and Remote Sensing* ,*41*(11), 2466–2477. doi:10.1109/tgrs.2003.817267

535 Maksud B., Claudia R., Anik B., Marc J. 2016. Optimizing irrigation efficiency improvements in
536 the Aral Sea Basin. *Water Resources and Economics*, 13: 30-45. doi: 10.1016/j.wre.2015.08.003

537 Micklin, P. 2007. The Aral Sea disaster. *Annual Review of Earth and Planetary Sciences*, *35*,
538 47–72. doi: 10.1146/annurev.earth.35.031306.140120

539 Micklin, P. 2016. The future Aral Sea: hope and despair. *Environmental Earth Sciences*, *75*(9),
540 1–5. doi: 10.1007/s12665-016-5614-5

541 Micklin, P. P. 1988. Desiccation of the Aral Sea: A water management Disaster in the Soviet
542 Union. *Science*, *241*(4870), 1170–1176. doi:10.1126/science.241.4870.1170

543 Micklin, P. 2010. "The past, present, and future Aral Sea.", *Lakes & Reservoirs: Research &*
544 *Management*, 15(3): 193-213, doi: 10.1111/j.1440-1770.2010.00437.x.

545 Parajuli, S. P. and Yang, Z. L. 2017. Understanding dust emission in the Bodélé region by
546 extracting locally mobilized dust aerosols from satellite Aerosol Optical Depth data using
547 principal component analysis. *Aeolian Research*, *24*, 105–113. doi: 10.1016/j.aeolia.2017.01.001

548 Philippe, S., Speranta, M. P., Stefan, K., Jean, P. S. and Hedi, O. 2007. Climate variability in the
549 Aral Sea basin (Central Asia) during the late Holocene based on vegetation changes.
550 *Quaternary Research*, *67*(3), 357–370. doi: 10.1016/j.yqres.2006.11.006

551 Saha S., Bovolo, F. and Bruzzone, L. 2019. Unsupervised Deep Change Vector Analysis for
552 Multiple-Change Detection in VHR Images.*IEEE Transactions on Geoscience*
553 *and Remote Sensing* ,*57*, 3677–3693, doi:10.1109/tgrs.2018.2886643

554 Schutz, B. E., Zwally, H. J., Shuman, C. A. and Hancock, D. 2005. Overview of the ICESat
555 Mission. *Geophysical Research Letters*, *32*(21), 97–116. doi:10.1029/2005GL024009

556 Shi H, Luo G, Zheng H, Chen C, Qlaf H, Bai J, Liu T, Liu S, Xue J, Cai P, He H, Uchenna F O,
557 Tim V, Philippe D. 2021. A novel causal structure-based framework for comparing a basin-wide
558 water–energy–food–ecology nexus applied to the data-limited Amu Darya and Syr Darya river
559 basins. *Hydrology and Earth System Sciences*, *25*(2):901-925, doi: 10.5194/hess-25-901-2021.

560 Shibuo, Yoshihiro, Jerker Jarsjö, and Georgia Destouni. 2007. "Hydrological responses to
561 climate change and irrigation in the Aral Sea drainage basin." *Geophysical Research
562 Letters,34*(21), doi: 10.1029/2007GL031465.

563 Singh, A., Seitz, F. and Schwatke, C. 2012. Inter-annual water storage changes in the Aral Sea
564 from multi-mission satellite altimetry, optical remote sensing, and GRACE satellite gravimetry.
565 *Remote Sensing of Environment*, *123*, 187–195. doi: 10.1016/j.rse.2012.01.001

566 Swenson, S. and Wahr, J. 2007. Multi-sensor analysis of water storage variations of the Caspian
567 Sea. *Geophysical Research Letters*, *34*(16), L16401. doi:10.1029/2007gl030733

568 Tewkesbury, A., Comber, A., Tate, N. J., Lamb, A. and Fisher, P. F. 2015. A critical synthesis of
569 remotely sensed optical image change detection techniques, *Remote Sensing of Environment*,
570 *160*, 1–14. doi: 10.1016/j.rse.2015.01.006

571 Tong, X., Brandt, M., Hiernaux, P., Herrmann, S.M., Feng, T., Prishchepov, A.V. and Fensholt,
572 R. 2017. Revisiting the coupling between NDVI trends and cropland changes in the Sahel
573 drylands: A case study in western Niger. *Remote Sensing of Environment*, *191*, 286–296. doi:
574 10.1016/j.rse.2017.01.030

575 Tucker, C. J. 1979. Red and photographic infrared linear combinations for monitoring
576 vegetation. *Remote Sensing of Environment*, *8*(2), 127-150. doi:10.1016/0034-4257(79)90013-0

577 Valentina, K. and Ladislav, H. 2009. Snow cover characteristics in the Aral Sea Basin from
578 different data sources and their relation with river runoff.*Journal of Marine Systems*, *76*(3), 254–
579 262. doi: 10.1016/j.jmarsys.2008.03.012

580 Wang, X. L., Luo, Y., He, C. S. and Liu, S. Y. 2016. Attribution of Runoff Decline in the Amu
581 Darya River in Central Asia during 1951–2007. *Journalof Hydrometeorology*, 17(5),1543–1560.
582 doi:10.1175/jhm-d-15-0114.1

583 Watkins, M. M., D. N. Wiese, D.-N. Yuan, C. Boening, and F. W. Landerer. 2015. Improved
584 methods for observing Earth's time variable mass distribution with GRACE using spherical cap
585 mascons. *Journal of Geophysical Research-Solid Earth*, *120*, doi:10.1002/2014JB011547.

586 Watts, L.M. and Laffan, S.W. 2014. Effectiveness of the BFAST algorithm for detecting
587 vegetation response patterns in a semi-arid region. *Remote Sensing of Environment*, *154*, 234–
588 245. doi: 10.1016/j.rse.2014.08.023

589 Wiese, D. N., F. W. Landerer, and M. M. Watkins. 2016. Quantifying and reducing leakage
590 errors in the JPL RL05M GRACE mascon solution, *Water Resources Research*, *52*, 7490–7502,
591 doi:10.1002/2016WR019344.

592 Wu, T., Sang, S., Wang, S., and Yang, Y. Y. 2020. Remote sensing assessment and
593 spatiotemporal variations analysis of ecological carrying capacity in the Aral Sea Basin. *Science
594 of the Total Environment*, *735*,139562. doi: 10.1016/j.scitotenv.2020.139562

595 Zhang, G. Q., Xie, H. J., Kang, S. C., Yi, D. H. and Ackley, S. F. 2011. Monitoring lake level
596 changes on the Tibetan Plateau using ICESat altimetry data (2003–2009). *Remote Sensing of*
597 *Environment*, *115*(7), 1733–1742. doi: 10.1016/j.rse.2011.03.005

598 Zhang, Y., Gao, J., Liu, L., Wang, Z., Ding, M. and Yang, X. 2013. NDVI-based vegetation
599 changes and their responses to climate change from 1982 to 2011: A case study in the Koshi
600 River Basin in the middle Himalayas. *Global and Planetary Change*, *108*, 139–148, doi:
601 10.1016/j.gloplacha.2013.06.012

602 Zheng W, Xu H Z, Zhong M, Yuan M J. 2009. Accurate and rapid error estimation on global
603 gravitational field from current GRACE and future GRACE Follow-On missions. *Chinese*
604 *Physics B*, *18*(8):3597-3604, doi: 10.1088/1674-1056/18/8/077.

605 Zhu, L. H., Liu, X. N., Wu, L., Tang, Y. B. and Meng, Y. Y. 2019. Long-Term Monitoring of
606 Cropland Change near Dong ting Lake, China, Using the LandTrendr Algorithm with Landsat
607 Imagery. *Remote Sensing*, *11*(10), 1234. doi: 10.3390/rs11101234

608 Zhu, Z. and Woodcock, C. E. 2012. Object-based cloud and cloud shadow detection in Landsat
609 imagery. *Remote Sensing of Environment*, *118*, 83–94. doi: 10.1016/j.rse.2011.10.028

610 Zwally, H. J., Yi, D. H., Kwok, R. and Zhao, Y. H. 2008. ICESat measurements of sea ice
611 freeboard and estimates of sea ice thickness in the Weddell Sea, *Journal of Geophysical*
612 *Research*, *113*(C2), C02S15, doi:10.1029/2007jc004284

Figure 1

Research scope
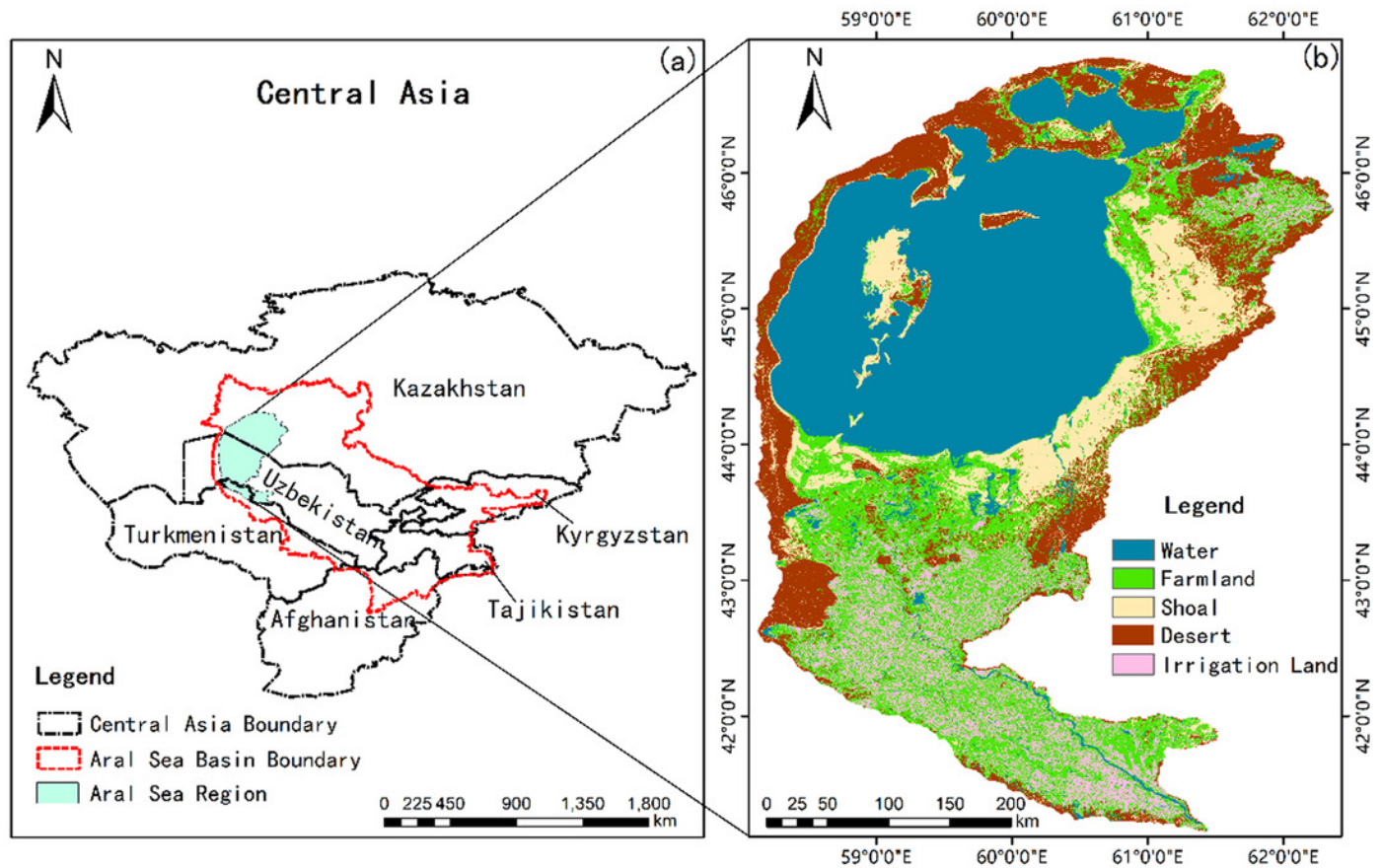
Figure 2

Research Method
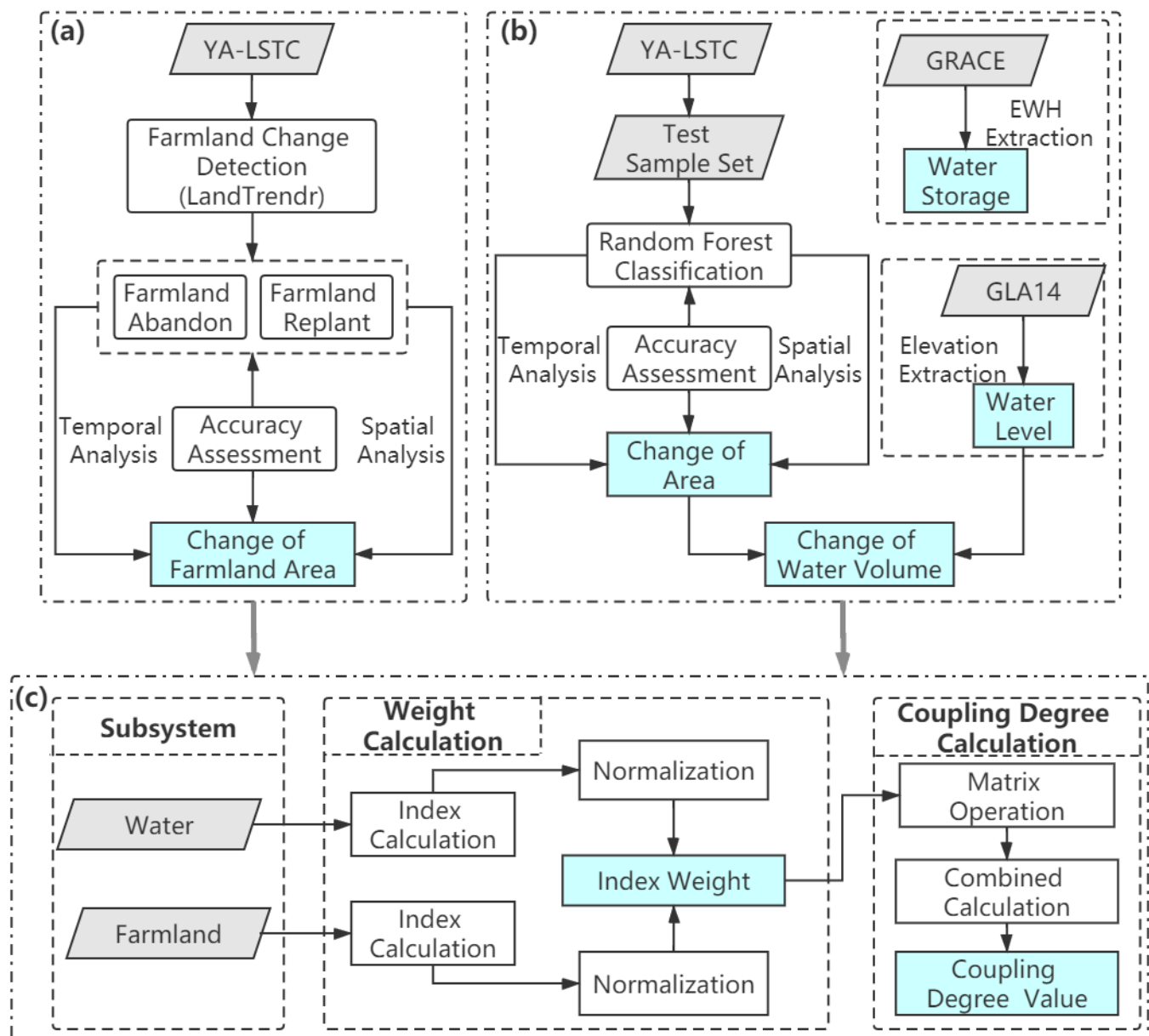
Figure 3

Examples areas of water change and farmland change near the Syr Darya and the Amu Darya. Figures a1 and a2 represent the water change years 2009 and 2019; Figures b1, b2, b3 represent the water change years 2009, 2016 and 2019
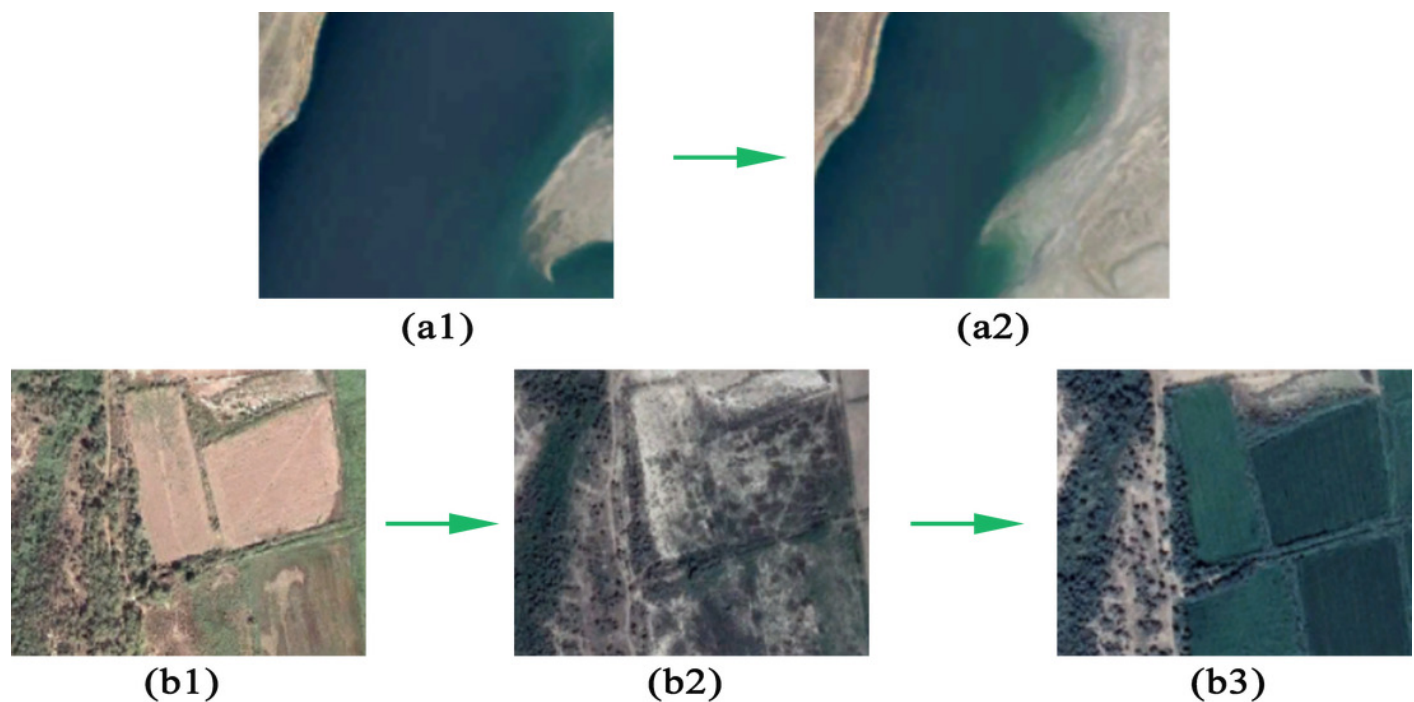
Figure 4

Year of abandoned farmland in the Aral Sea Region with two areas shown in detail
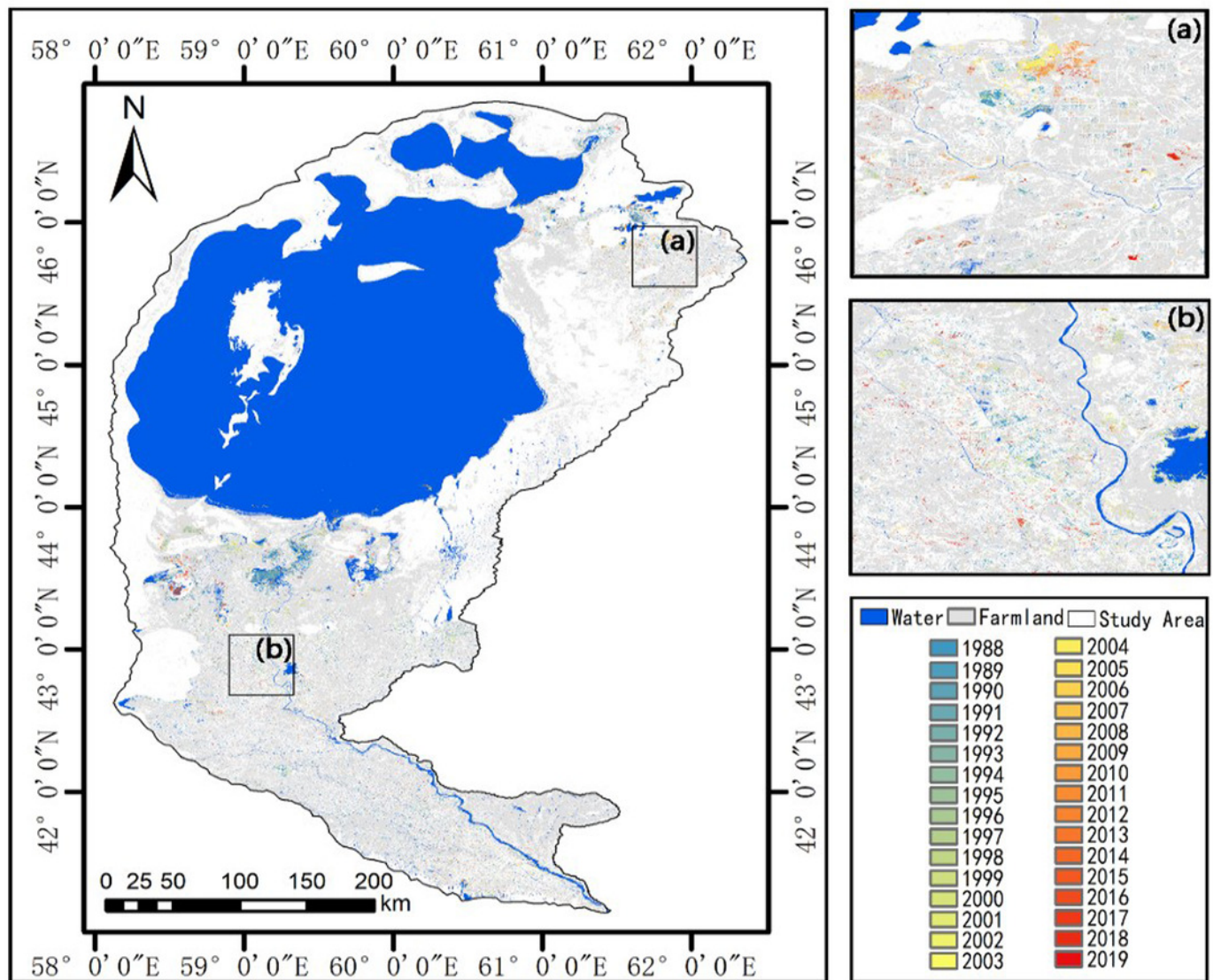
Figure 5

Change of the Aral Sea area from 1987 to 2019
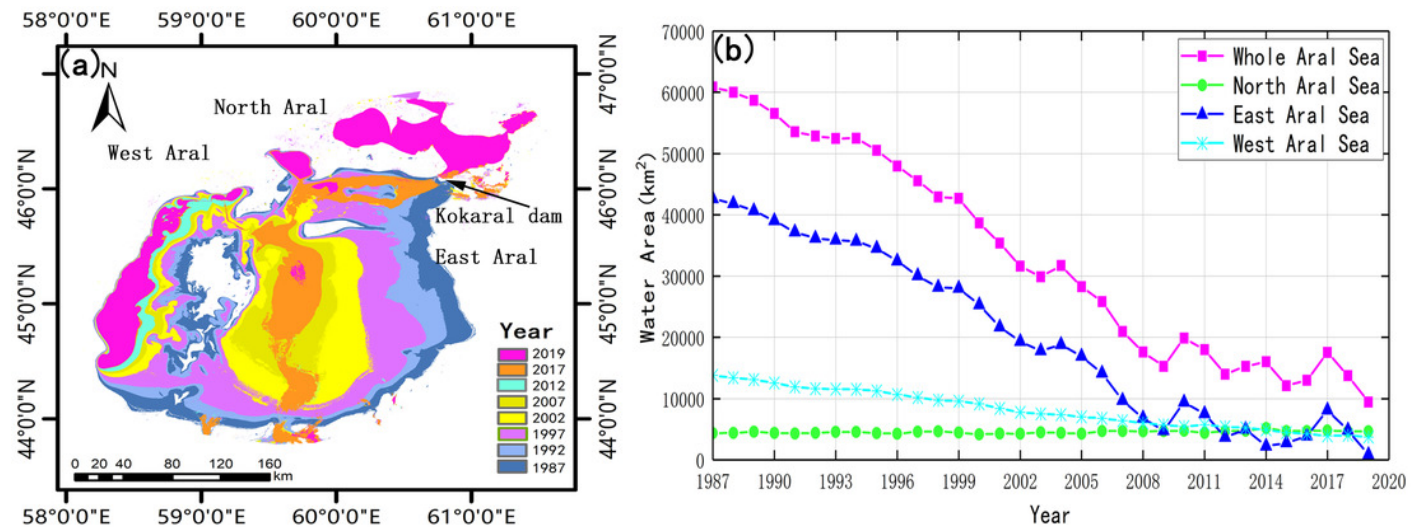
Figure 6

Change of the Aral Sea water level from 2003 to 2009

Figure 7

Mass change of the Aral Sea Region from 2002 to 2016